Time series analysis of turbulent and non-autonomous systems

Philip Clemson and Aneta Stefanovska

Department of Physics, Lancaster University, Lancaster, United Kingdom

Abstract. Time series analysis is commonly applied to both chaotic and stochastic systems, which are collectively described as turbulence. However, explicitly time-dependent non-autonomous systems can also generate turbulent dynamics, which makes them useful for describing many physical phenomena. Nevertheless, many of the methods used to analyse turbulence are based around autonomous systems. In this paper, time series from the chaotic, stochastic and non-autonomous Duffing system are analysed using these methods to gauge their suitability to non-autonomous systems. It is found that time-dependent representations are vitally important in the study of this class of systems. Moreover, when time-dependence is neglected in the representation a completely deterministic non-autonomous system is often indistinguishable from a stochastic system.

Keywords: turbulence, chaos, stochastic, embedding, wavelet transform, complexity, quasi-periodic forcing
PACS: 05.10.-a,05.40.-a,05.45.-a,05.45.Tp

INTRODUCTION

The concept of turbulence originated in the field of fluid dynamics from the work of Stokes and Reynolds [1, 2] with later developments by Kolmogorov and others [3, 4, 5]. Though it is still largely associated with this field, turbulent dynamics have grown to become a unifying theory of systems not only in physics but in chemistry, biology, meteorology and many other areas.

It therefore seems that the phenomenon has outgrown its original application to high-dimensional spatio-temporal systems and consequently requires a more general definition. In this paper we define turbulence as any system that is far from thermodynamic equilibrium, exhibiting a large, complex distribution of states.

Using this definition, turbulence can be generated through several distinct mechanisms. Perhaps the most well known and studied of these is chaos, where the turbulent dynamics originate from the exponential growth of small perturbations in the system [6]. Another well-studied class are stochastic systems, where the external forcing by noise is the cause [7]. However, a third class is also able to produce turbulent dynamics and is currently the subject of much debate: non-autonomous systems [8].

Non-autonomous systems are defined as being explicitly dependent on time. The most easily understood forms are transient systems, where the invariant properties of the system are clearly time-dependent. However, even stable systems can be non-autonomous if the defining mechanism of the dynamical equations contain any solely time-dependent variables which do not rely on the internal dynamics of the system.

In the same way as chaos, turbulence in non-autonomous systems can arise without

the need for external noise. As will be seen, setting the time-dependent variable as a fully deterministic quasi-periodic function is enough to generate non-chaotic turbulence in a nonlinear oscillator.

Duffing oscillator

The unforced Duffing oscillator is a 2-dimensional system with a cubic nonlinearity. It is defined by the differential equation

$$\frac{d^2x}{dt^2} + \delta\frac{dx}{dt} + \beta x + \alpha x^3 = 0, \tag{1}$$

where α, β and δ are constants. Here we choose $\alpha = 1$ and $\beta = -1$. The second dimension is denoted by $y = \frac{dx}{dt}$.

The equation was originally investigated by Georg Duffing who was studying the real-world vibrations it could describe [9]. The equation has since been applied and adapted to produce many different types of dynamics, which are comprehensively described in the book by Kovačić and Brennan [10]. For $\beta < 0$ the trajectory of the unforced system orbits two fixed points located on the line $y = 0$ at equal distances from $x = 0$. For $\delta > 0$ the system is damped, which means the amplitude of the oscillations reduces over time and eventually settles at one of the fixed points. However, this damping effect can be offset by external forcing of the system, which can in turn lead to turbulence.

One of the most widely known forms of the forced Duffing system is when it is periodically forced,

$$\frac{d^2x}{dt^2} + \delta\frac{dx}{dt} - x + x^3 = \gamma\cos(\omega t), \tag{2}$$

where γ and ω are constants. This added term gives rise to chaos, which was originally discovered by Yoshisuke Ueda [11, 12]. Ueda used $\delta = 0.2$, $\gamma = 0.3$ and $\omega = 1$, which we adopt here.

Another version of the system is the noise-forced case,

$$\frac{d^2x}{dt^2} + \delta\frac{dx}{dt} - x + x^3 = \xi\eta, \tag{3}$$

where $\eta(t)$ is a normalized Gaussian white noise variable and $\xi = \sqrt{2D_n}$ is a constant where D_n is the noise intensity; in this case $\xi = 0.2$ is chosen. With the addition of this noise term, the system is transformed into a non-deterministic (stochastic) oscillator, where the apparent randomness of the dynamics originates from an external source. This form of the Duffing system is also famous for exhibiting a phenomenon known as stochastic resonance [13], which is a term for the large fluctuations in the dynamics that result from random switching between orbits around the two fixed points.

A third possibility which has not been studied to the extent of the previous two examples is the quasi-periodically forced system,

$$\frac{d^2x}{dt^2} + \delta\frac{dx}{dt} - x + x^3 = \gamma\left(\sin(2\pi\omega_1 t) + \sin(\omega_2 t)\right). \tag{4}$$

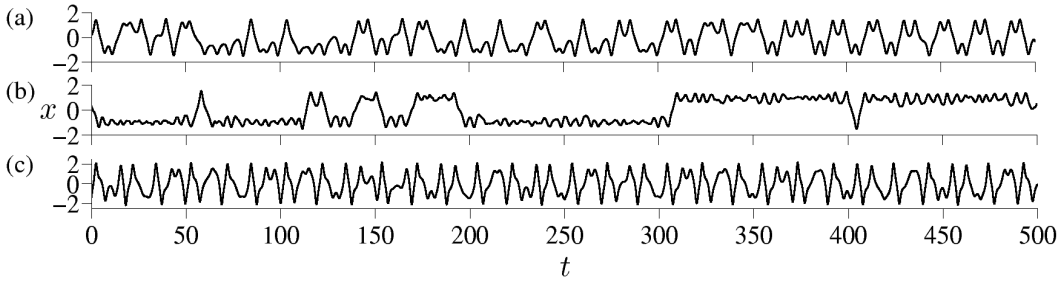

FIGURE 1. Time series of the three test systems from $t = 0$ to $t = 500$: (a) Chaotic; (b) Stochastic; (c) Non-autonomous.

Here the ratio of the frequencies $2\pi\omega_1/\omega_2$ is an irrational number. This means that while the forcing term is fully deterministic, it is not periodic. The attractor is therefore explicitly time-dependent[1], as opposed to the periodically forced version of the system (2) where the position of the trajectory can be plotted at intervals of $t = t_o, t_o + 2\pi/\omega, t_o + 4\pi/\omega, \ldots$ to find the attractor for a particular phase of $\cos(\omega t)$. The quasi-periodically forced system can therefore be categorised as a non-autonomous system.

Numerical integration

The test time series are generated using the Heun scheme:

$$\begin{aligned} \tilde{x}_{n+1} &= x_n + hf(t_n, x_n), \\ x_{n+1} &= x_n + \frac{h}{2}\left(f(t_n, x_n) + f(t_{n+1}, \tilde{x}_{n+1})\right), \\ \frac{dx}{dt} &= f(t, x), \end{aligned} \tag{5}$$

where the step $h = 10^{-3}$ is used. For the stochastic system the algorithm is adjusted according to Honeycutt [14] to account for the noise term.

Each of the time series are integrated from $t = 0$ to $t = 10000$, samples of which are shown in Figure 1.

PHASE SPACE ANALYSIS

Phase space representations are very useful for understanding the dynamics of non-linear systems and identifying invariant properties such as the exponents developed by Aleksandr Lyapunov [15] and the attractor dimensions as defined by Alfred Rényi [16, 17, 18]. The downside of these kind of representations is that when the conversion to phase space has been made it is no longer possible to separate the purely time-dependent (non-autonomous) parts of the system from the time-independent (autonomous) parts.

---

[1] Note however that this time-dependence is still defined by a stationary term.

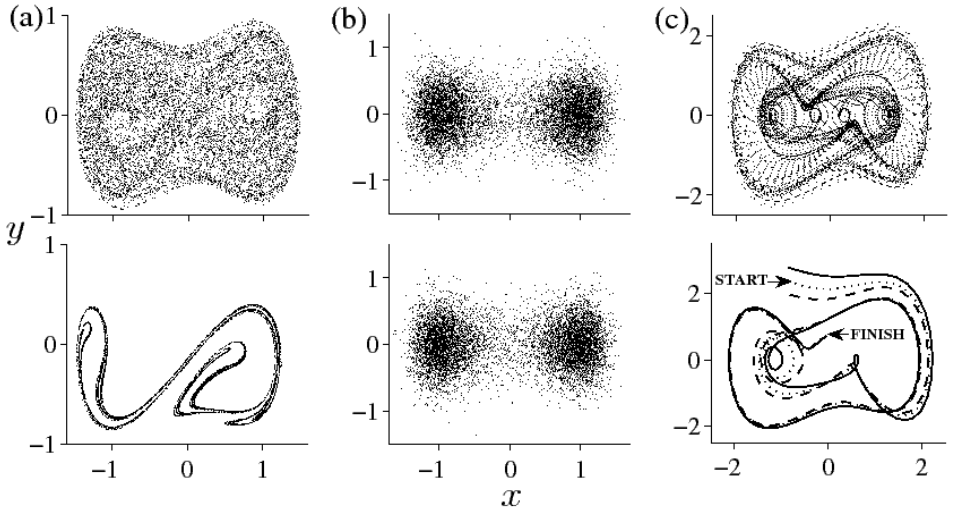

FIGURE 2. Phase space representations of the forced Duffing system: (a) Chaotic; (b) Stochastic; (c) Non-autonomous. Shown above are the attractors as seen by removing the time axis from a single trajectory of the system. Shown below for (a) and (b) are the last points of 10,000 trajectories with different initial conditions, which were integrated over a period $t_{\mathrm{f}} - t_{\mathrm{o}} = 100$. Shown below (c) is the evolution of three trajectories with different initial conditions from $t_{\mathrm{o}} = 0$ to $t_{\mathrm{f}} = 20$.

Figure 2 shows phase portraits of the three versions of the forced Duffing system in the $x - y$ plane. The fractal structure of the attractor for the chaotic system is lost in the time-independent form, although in both cases the states are spread out across a large area of phase space. On the other hand, both representations are the same for the stochastic system, where the Markovian dynamics cause the attractor to be essentially time-independent.

However, for the non-autonomous system the two representations are the most dissimilar. In the time-independent form the states are spread out across phase space in the same way as the chaotic and stochastic systems. In contrast, the time-dependent form is in fact a singularity which all trajectories converge to, due to the fact that the global Lyapunov exponent of the system is negative. This significant inconsistency leads to a fundamental misrepresentation of non-autonomous systems in phase space analysis.

Time delay embedding theorem

The process of transforming a time series $x(t)$ into phase space is known as *embedding*. The framework of this transformation was developed by Floris Takens [19] and Ricardo Mañé [20] and involves the construction of an embedding vector for each point in time:

$$\mathbf{x}(t_i) = [x(t_i), x(t_i + l\Delta t), \ldots, x(t_i + (d_e - 1)l\Delta t)], \tag{6}$$

where d_e is the *embedding dimension* and l is an integer, both of which must be chosen prior to embedding. For d_e, the embedding theorem states that in order to correctly

reconstruct the system in phase space for any l, the following condition must be met:

$$d_e \geq 2D+1, \tag{7}$$

where D is the smallest theoretical dimension of phase space for which the trajectories of the system will not overlap [21].

Estimation of $l\Delta t$

A problem with the embedding theorem is that it does not specify any conditions for the value of l. However, in practice it is necessary to have a delay that maximizes the spread of the data in phase space [22, 23].

In general, the best time delays are neither extremely short, which causes the values in the embedding vectors to be essentially the same, or extremely large, which means the values become uncorrelated random variables [24]. The method devised by Fraser and Swinney which uses the idea of mutual information [25] is commonly used to estimate this ideal time delay. For the time series $x(t)$ starting at t_o and the delayed time series $x_d(t)$ starting at $t_o + l\Delta t$ the mutual information is given by

$$I(l\Delta t) = \sum_{i=1}^{N-l} P_{xx_d}(x(t_i), x_d(t_i)) \log_2 \left(\frac{P_{xx_d}(x(t_i), x_d(t_i))}{P_x(x(t_i)) P_{x_d}(x_d(t_i))} \right), \tag{8}$$

where P_x and P_{x_d} are the probability distributions for $x(t)$ and $x_d(t)$ respectively and P_{xx_d} is the joint probability distribution (the probability of observing a value from one time series and a value from the other at the same time). The local minima in $I(l\Delta t)$ provide values of l which maximise the spread of the trajectory in phase space.

The problem with this method, and indeed the other estimators of l, is that there are often several minima in $I(l\Delta t)$ that can be chosen. As already stated, the first minimum is usually said to be the most appropriate choice since it maintains some correlation between the dimension variables. However, no matter which choice is made the dynamics corresponding to timescales smaller than the chosen delay will appear as noise, which means that some information will inevitably be lost in embedding.

Estimation of d_e

The condition given in (7) has little meaning when applied to observed time series where D is not known. For this purpose, the method of false nearest neighbours was developed as a way of estimating the dimension [26]. For a given d_e, each embedding vector is paired with its nearest neighbour, i.e. the one separated by the smallest Euclidean distance R_{d_e}:

$$\begin{aligned} R_{d_e} =& ([x(t_i) - x(t_{NN})]^2 + [x(t_i + l\Delta t) - x(t_{NN} + l\Delta t)]^2 + \dots \\ & \dots + [x(t_i + (d_e - 1)l\Delta t) - x(t_{NN} + (d_e - 1)l\Delta t)]^2)^{\frac{1}{2}}, \end{aligned} \tag{9}$$

where t_{NN} is the position of the nearest neighbour in the time domain. A new embedding dimension $d_e + 1$ is then used and R_{d_e+1} is now calculated for the same vectors that were identified as nearest neighbours in the previous embedding. If $(R^2_{d_e+1} - R^2_{d_e})/R^2_{d_e}$ is greater than some threshold value R^2_T then the vector pair are labelled as *false* nearest neighbours. The choice of R_T is entirely subjective although others have stated that the algorithm performs well for $10 \leq R_T \leq 30$ [26, 27]. If the percentage of false nearest neighbours is high (typically $> 1\%$ [26]) this implies that other dimensions have been projected onto the d-dimensional phase space, causing points that would otherwise be completely separate to appear close together. The procedure can then be repeated for $d_e + 1, d_e + 2, \ldots$ until the percentage of false nearest neighbours is sufficiently small so that the embedding dimension satisfies a similar condition to (7).

As will be seen, the main issue when estimating the embedding dimension is that time-dependent *non-autonomous* terms (including noise) are interpreted as extra *autonomous* dimensions. At present, the time-delay embedding framework has no way of distinguishing between the dynamics making up the invariant autonomous attractor of the system and the purely time-dependent effects.

Correlation integral

One of the most widely used phase space measures is the correlation dimension D_2. An algorithm created by Grassberger and Procaccia [28, 29] may be used to estimate the dimension directly from the embedded time series. This begins with the computation of the correlation integral,

$$C(\varepsilon) = \frac{1}{N(N-1)} \sum_{i=1}^{n_v} \sum_{\substack{j=1 \\ j \neq i}}^{n_v} H(\varepsilon - ||\mathbf{x}(t_i) - \mathbf{x}(t_j)||), \tag{10}$$

where H is the Heaviside step function and n_v is the number of embedding vectors. This integral is simply a sum of the number of "neighbouring" embedding vectors, defined as those that have an absolute distance $\leq \varepsilon$. The correlation dimension is then defined as:

$$D_2 = \lim_{\varepsilon \to 0} \lim_{N \to \infty} \frac{d(\ln C(\varepsilon))}{d(\ln \varepsilon)}. \tag{11}$$

In practice the value of D_2 is estimated as the plateau where $\frac{d(\ln C(\varepsilon))}{d(\ln \varepsilon)}$ stays constant as $\ln \varepsilon$ decreases. However, $C(\varepsilon)$ is dependent on the embedding dimension d_e, so in order to check the stability of the estimate for D_2 the integral must be recalculated for several embeddings.

Figure 3 shows the correlation integrals for the three test systems. The plateau identifies a dimension $D_2 \approx 2.4$ for the attractor of the chaotic system, which is reasonable since the attractor in Figure 2 appears to be approximately 2-dimensional. For the stochastic system there is instability around the estimated embedding dimension because the stochastic dynamics fill any new dimensions, which means a finite dimension cannot be defined.

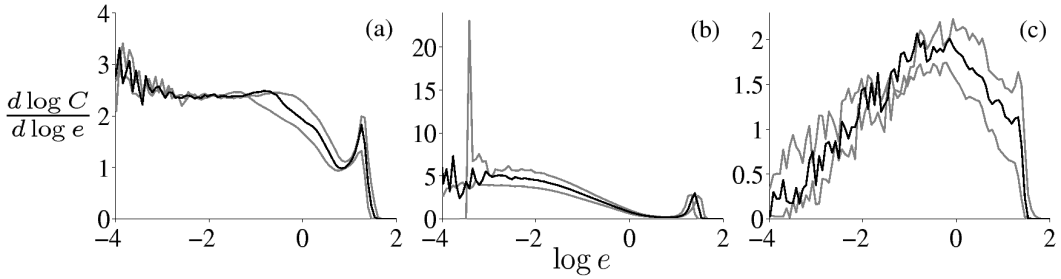

FIGURE 3. Correlation integrals for the embedding dimension d_e estimated by the false nearest neighbours algorithm (black) as well as for $d_e \pm 1$ (grey): (a) Chaotic system; (b) Stochastic system; (c) Non-autonomous system.

The method is also unable to find a stable plateau in D_2 for the non-autonomous system. The embedding is in fact including the dynamics of the external forcing in the autonomous attractor, in the same way that new dimensions are filled with noise in the stochastic system. The correlation dimension is therefore also difficult to define in non-autonomous systems.

Karhunen-Loève decomposition

The time-delay embedding theorem is also applied in the Karhuen-Loève expansion, also known as principal value decomposition [30, 31]. The first step is to compute the correlation matrix of the embedded time series [32],

$$\mathbf{C} = \mathbf{x}^T \mathbf{x}, \tag{12}$$

with eigenvectors $\mathbf{v_i}$ and eigenvalues λ_i given by:

$$\mathbf{C}\mathbf{v}_i = \lambda_i \mathbf{v}_i. \tag{13}$$

The eigenvectors are used to form the rows of a new matrix $\mathbf{V}$ and are ordered with respect to the size of the corresponding eigenvalues, i.e. so that the eigenvector with the largest eigenvalue makes up the first row of $\mathbf{V}$, the one with the second largest makes up the second row and so on. The ith mode of the time series decomposition is then given by $\hat{\mathbf{x}}_i = \mathbf{H}_i \mathbf{V}_i^T$ where $\mathbf{H}_i$ is the ith row of the matrix

$$\mathbf{H} = \mathbf{x}\mathbf{V}^T \tag{14}$$

and $\mathbf{V}_i$ is the corresponding row of the matrix $\mathbf{V}$. The number of modes is equal to the embedding dimension d_e, with the first mode $\hat{\mathbf{x}}_1$ representing the component with the most energy in the time series. The application of Karhunen-Loève decomposition to the three test systems is shown in Figure 4. There appears to be very little dependence on the embedding dimension for eigenvalues of the chaotic system, where the distribution simply becomes flatter in each case. However, for the stochastic and non-autonomous systems the distribution of eigenvalues changes in structure for each new embedding,

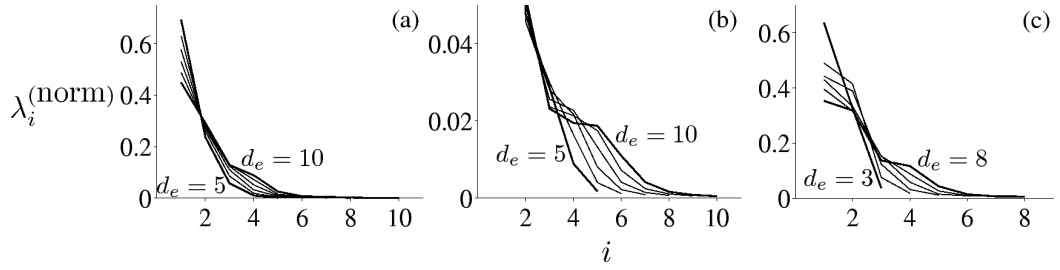

FIGURE 4. Eigenvalues from Karhunen-Loève decomposition for different embedding dimensions: (a) Chaotic system; (b) Stochastic system; (c) Non-autonomous system. In each case the eigenvalues have been normalised by dividing by the sum over all of the eigenvalues.

even after an increase of 5 dimensions. Again, this demonstrates how the time-delay embedding method is unable to cope with non-autonomous dynamics. It is also apparent that by using phase space analysis it is easy to mistake a non-autonomous system for a stochastic one.

FOURIER TRANSFORM

One of the most widely-used forms of time series analysis is the discrete Fourier transform (DFT), which was first developed by Carl Friedrich Gauss around 1805 [33][2]. It is defined as:

$$F(\omega) = \sum_{n=0}^{L-1} f(n) e^{-\frac{2\pi i \omega n}{L}}, \tag{15}$$

where L is the number of points in the time series $f(n)$. The complex Fourier basis $e^{-\frac{2\pi i \omega n}{L}}$ contains a sine and cosine function which resolve the amplitude and phase of the stationary periodic components at each frequency ω. A common convention is to present the square of the Fourier transform, which gives the *power* of the Fourier components:

$$P(\omega) = |F(\omega)|^2. \tag{16}$$

The DFT transforms a time series from the time domain to the frequency domain. The transformation is therefore similar to the time-delay embedding method in the way that it removes the time-dependent effects from the data. This becomes a problem when dealing with non-stationary time series (whether chaotic, stochastic or non-autonomous) where the properties of the Fourier components change with time. As can be seen in Figure 5, the completely deterministic oscillations appear indistinguishable from the stochastic oscillation.

Figure 5 shows Fourier transforms of time series from the three turbulent systems. The Fourier components have a continuous (although nonuniform) distribution for the

[2] Gauss' research was motivated by work to determine the orbits of asteroids by analysing time series of their locations and predates the publication of Joseph Fourier's work on the continuous Fourier transform.

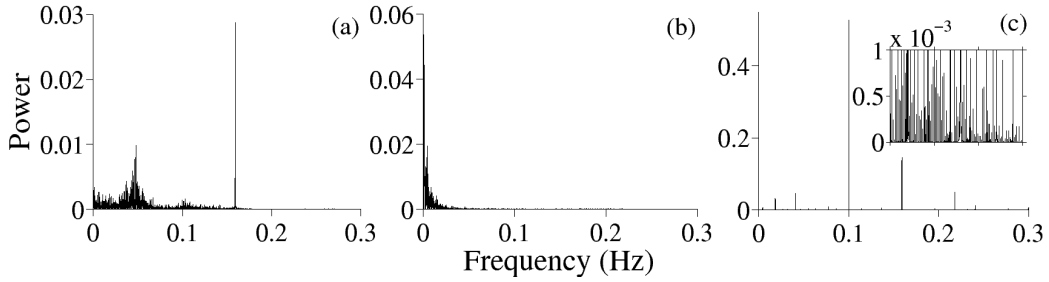

FIGURE 5. Fourier transforms over the range 0-0.3Hz (using seconds for the units of t) for: (a) Chaotic system; (b) Stochastic system; (c) Non-autonomous system with another plot showing detail over the same range of frequencies.

chaotic and stochastic systems, which indicates that the time series are not periodic. The largest spikes in the spectra of the chaotic and non-autonomous systems correspond to the sinusoidal components of the forcing terms. The other spikes in the Fourier transform of the non-autonomous system are more ambiguous and in fact the low-power Fourier components are spread across a wide range of frequencies in the same fashion as the chaotic and stochastic systems.

Since all three of the time series analysed are non-stationary, the frequency domain representation provided by the Fourier transform is unclear. Apart from the sinusoidal forcing components, it is difficult to understand the physical meaning of the Fourier components. Hence, in the same way as phase space analysis, the removal of time has resulted in ambiguity in the interpretation of three systems.

COMPLEXITY ANALYSIS

The complexity of a time series is used to describe the amount of disorder or 'roughness'. The idea is related to fractal dynamics, where the normalised structure over short timescales resembles the normalised structure over larger timescales. A high *fractal symmetry* means that the shape of the time series as defined by fast fluctuations at small scales will appear similar to the shape defined by slow fluctuations at large scales. Simple time series such as a single sine wave have the least fractal symmetry, whereas more noisy signals with many components have a high fractal symmetry, which consequently makes this property a good measure of complexity.

A widely used measure of fractal scaling is the fractal *dimension*, D_F. It is defined as the exponent which dictates the number of similar structures n_s at a scale ε contained within a larger similar structure,

$$n_s \propto \varepsilon^{-D_F}. \tag{17}$$

High fractal dimensions therefore correspond to very 'rough' time series, where the repeated fractal structure contains a lot of detail.

The standard way of measuring fractal symmetry in a time series and to estimate D_F is with detrended fluctuation analysis (DFA) as introduced by Peng et al. [34]. This

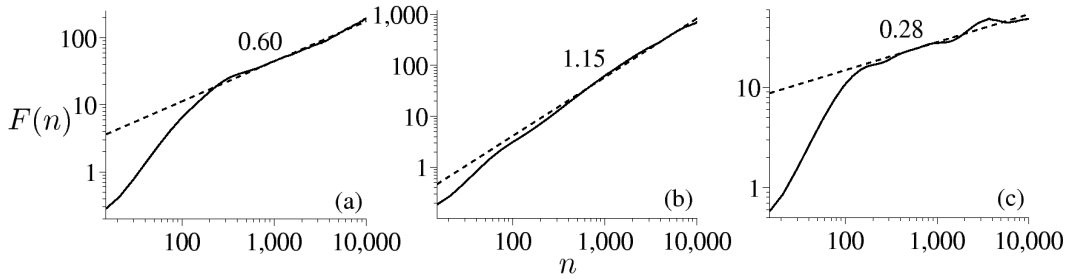

FIGURE 6. Detrended fluctuation analysis of time series from the three turbulent systems: (a) Chaotic system; (b) Stochastic system; (c) Non-autonomous system. The numbers show the values for α calculated from linear fits (dashed lines).

estimates the self-similarity parameter α, which is defined in the equation,

$$X(t) \equiv a^{\alpha} X\left(\frac{t}{a}\right), \tag{18}$$

where $X(t)$ is the time series integrated over time (calculated by the cumulative addition of successive points) and a is the scaling or magnification factor.

In order to estimate α the time series is divided into sections of length n. For each section the local trend is removed by subtracting a fitted polynomial (usually of first order [35, 34]). The root mean square *fluctuation* for the scale equal to n is then given by,

$$F(n) = \sqrt{\frac{1}{N}\sum_{i=1}^{N} Y_n(t_i)^2}, \tag{19}$$

where $Y(t)$ is the integrated and detrended time series. The fluctuation $F(n)$ provides a measure of the amplitude at the corresponding scale which should follow the same scaling as in (18). By plotting $\log F(n)$ against $\log n$, the self-similarity parameter α is then given by the gradient of the line. The relation between the DFA exponent and the fractal dimension of the time series is given by $D_F = 3 - \alpha$ for $1 < \alpha < 2$ [36].

Detrended fluctuation analysis of the three time series is shown in Figure 6. The first slope that occurs at small timescales corresponds to the main oscillatory component and can be disregarded. For the chaotic system the value of α for the second slope implies that the direction of fluctuations in $X(t)$ are neither persistent nor anti-persistent, with dynamics that appear similar to white noise. For the stochastic system the exponent is determined to be $\alpha = 1.15$, which is the same as found for correlated noise [35]. However, for the non-autonomous system the scaling of the fluctuations generates a bumpy slope, which makes it difficult to define α. The simple time-dependent point attractor of this system should result in an exponent $\alpha \ll 0.5$, which would indicate a high degree of stability (anti-persistence in the direction of fluctuations). For the linear fit applied in Figure 6 the value $\alpha = 0.28$ seems to agree, although higher values could also be found by using other parts of the slope.

WAVELET TRANSFORM

The previous time series analysis methods have been shown to produce ambiguous results when applied to a non-autonomous system. The main contributing factor in each case is that the time-dependent properties have been removed from the representation of the system, resulting in the external non-autonomous components being included in the autonomous dynamics of the system.

While there is currently no time-dependent embedding method, the Fourier transform does indeed have a time-dependent counterpart known as the *wavelet transform* [37].

Wavelets have been developed to give "optimal" time-frequency resolution which is achieved by using an adaptive window. The continuous wavelet transform is defined by

$$W(s,t) = \int_{-L/2}^{L/2} \Psi(s,u-t) f(u) du, \tag{20}$$

where $\Psi(s,u)$ is known as the mother wavelet, which is scaled according to the parameter s to change its frequency distribution and time-shifted according to the parameter u. Rather than computing a "stand-alone transform" for each time window, the wavelet transform performs a different calculation depending on both time *and* frequency (or more specifically, the scale s). This means a new wavelet and window size is used to calculate each scale, with a small wavelet / window for high frequencies and larger ones for low frequencies. Individual oscillations can then be picked out continuously in both frequency and time.

In order to make direct comparisons with the Fourier transform, the Morlet wavelet must be used,

$$\Psi(s,u) = s^{-1/2} e^{-\frac{u^2}{2s^2}} e^{-\frac{2\pi i \omega_c u}{s}}, \tag{21}$$

where $s = 1/\omega$. The parameter ω_c is the center frequency, which determines the time-frequency resolution of the wavelet ($\omega_c = 1$ is used in this case). The $s^{-1/2} e^{-\frac{u^2}{2s^2}}$ part specifies the Gaussian shape of the window and stretching of the wavelet with respect to s while $e^{-\frac{2\pi i \omega_c u}{s}}$ is equivalent to the basis of the Fourier transform.

Figure 7 shows the wavelet transforms of the three systems. For the chaotic and stochastic systems a random distribution of oscillations at varying frequencies is seen. However, for the non-autonomous system the oscillations appear much more confined within the time-frequency plane, with a deterministic structure. In addition, the components corresponding to the spikes in Figure 5 are in fact correlated in time, which means that they are simply harmonics of a single deterministic oscillation. The true nature of the non-autonomous system is therefore easily identified with the wavelet transform.

CONCLUSION

In this paper we have commented on the analytical framework for the class of turbulent non-autonomous systems which are often overlooked. Many time series analysis methods do not take into account the possibility of this class of systems, which means that the corresponding time series can be indistinguishable from a stochastic system.

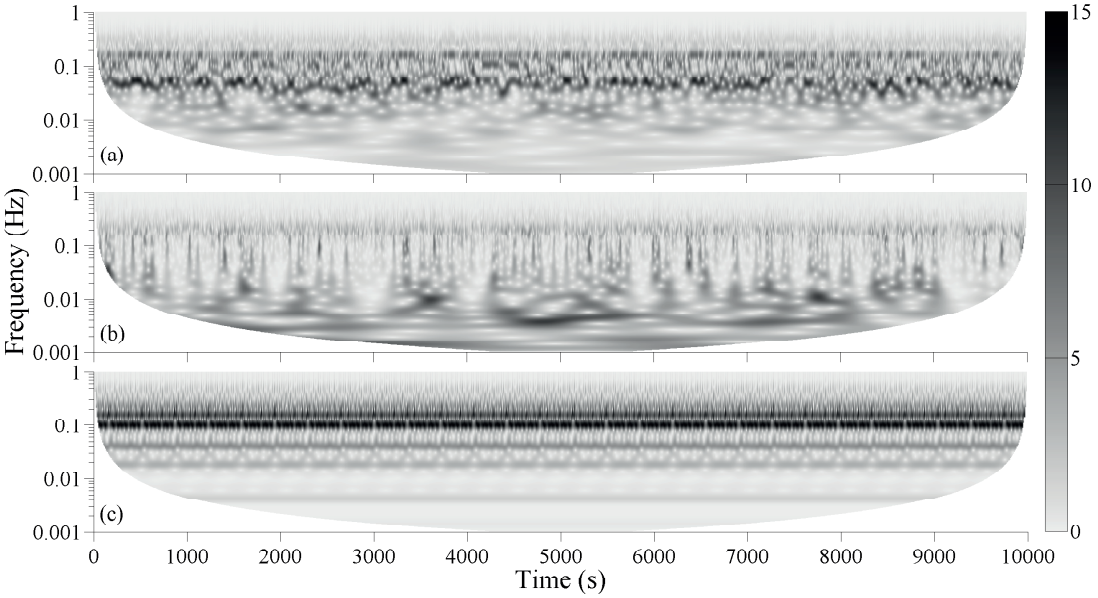

FIGURE 7. Amplitude of the continuous wavelet transform of time series from the three test systems: (a) Chaotic system; (b) Stochastic system; (c) Non-autonomous system. The wavelet transform expands the plots shown in Figure 5 to include the variations of the spectrum in time, where the peaks correspond to individual oscillations at a specific time and frequency. The scale is also logarithmic so that the detail at the lower frequencies can be seen more clearly. The white space at the edges of the time-frequency plane is where the wavelet time window extends beyond the ends of the time series, giving rise to a 'cone of influence'.

As has been emphasised throughout the analysis of the test systems, the solution is to include time in all representations of turbulent systems. This is of particular importance in inverse problems, where it may not be known if the system contains a non-autonomous component. The wavelet transform is one such method which meets this criteria but other tools have also been developed such as bispectral analysis [38, 39], harmonic detection [40], windowed phase coherence [41] and Bayesian inference [42]. However, non-autonomous systems still lack a characterisation similar to that offered by phase space via the time-delay embedding theorem. Finding a technique to reconstruct the autonomous part of the attractor from a single time series remains an unsolved problem.

ACKNOWLEDGMENTS

The research presented in this paper was supported by the Engineering and Physical Sciences Research Council (EPSRC).

REFERENCES

1. G. Stokes, *Trans. Camb. Phil. Soc.* **9**, 8–106 (1851).
2. O. Reynolds, *Phil. Trans. R. Soc.* **174**, 935–982 (1883).
3. A. Kolmogorov, *Dokl. Akad. Nauk SSSR* **31**, 301–305 (1941).

4. B. Eckhardt, T. M. Schneider, B. Hof, and J. Westerweel, *Annu. Rev. Fluid Mech.* **39**, 447–468 (2007).
5. P. S. Landa, *Europhys. Lett.* **36**, 401–406 (1996).
6. S. H. Strogatz, *Nonlinear Dynamics and Chaos*, Perseus Books Publishing, Cambridge, MA, USA, 1994.
7. F. Moss, and P. V. E. McClintock, *Noise in Nonlinear Dynamical Systems: Vol. 1, Theory of Continuous Fokker-Planck Systems*, Cambridge University Press, Cambridge, 1989.
8. P. E. Kloeden, and M. Rasmussen, *Nonautonomous Dynamical Systems*, American Mathematical Soc., 2011.
9. G. Duffing, "Erzwungene Schwingungen bei veränderlicher Eigenfrequenz und ihre technische Bedeutung.," in *Issues 41-42 of Sammlung Vieweg*, F. Vieweg & sohn, 1918.
10. I. Kovačić, and M. J. Brennan, *The Duffing Equation: Nonlinear Oscillators and Their Behaviour*, John Wiley & Sons, Chichester, UK, 2011.
11. Y. Ueda, *J. Stat. Phys.* **20**, 181–196 (1979).
12. Y. Ueda, *Nonlin. Dyn.* **357**, 422–434 (1980).
13. N. Li-Juan, X. Wei, and Y. Ming-Li, *Chinese Phys. B* **17**, 486–491 (2008).
14. R. L. Honeycutt, *Phys. Rev. A* **45**, 600–603 (1992).
15. A. M. Lyapunov, *The General Problem of the Stability of Motion*, Ph.D. thesis, Moscow University (1892), (translated into English by A. T. Fuller, *Int. J. Control* **55**, 531–773 (1992)).
16. J. Balatoni, and A. Rényi, "On the notion of entropy," in *Selected papers of Alfred Rényi, vol. I*, Akademiat Kiado, Budapest, 1976, pp. 558–584.
17. A. Rényi, *Acta Math. Acad. Sci. Hung.* **10**, 193–215 (1959).
18. A. Rényi, "Dimension, entropy and information," in *Trans. 2nd Prague Conf. Information Theory*, Czechoslovak academy of Sciences, Prague, 1960, pp. 545–556.
19. F. Takens, "Detecting strange attractors in turbulence," in *Dynamical Systems and Turbulence, Lecture Notes in Mathematics*, Springer-Verlag., 1981, vol. 898, p. 366Ű381.
20. R. Mañé, "On the dimension of the compact invariant sets of certain non-linear maps," in *Dynamical Systems and Turbulence, Lecture Notes in Mathematics*, Springer-Verlag., 1981, vol. 898, pp. 230–242.
21. H. D. I. Abarbanel, R. Brown, J. J. Sidorowich, and L. S. Tsimring, *Rev. Mod. Phys.* **65**, 1331–1392 (1993).
22. M. Small, *Applied Nonlinear Time Series Analysis: Applications in Physics, Physiology and Finance*, World Scientific, Singapore, 2005.
23. H. S. Kim, R. Eykholt, and J. D. Salas, *Physica D* **127**, 48–60 (1999).
24. R. Brown, P. Bryant, and H. D. I. Abarbanel, *Phys. Rev. A* **43**, 2787–2806 (1991).
25. A. M. Fraser, and H. L. Swinney, *Phys. Rev. A* **33**, 1134–1140 (1986).
26. M. B. Kennel, R. Brown, and H. D. I. Abarbanel, *Phys. Rev. A* **45**, 3403–3411 (1992).
27. C. Rhodes, and M. Morari, *Phys. Rev. E* **55**, 6162–6170 (1997).
28. P. Grassberger, and I. Procaccia, *Phys. Rev. Lett.* **50**, 346–349 (1983).
29. P. Grassberger, and I. Procaccia, *Physica D* **9**, 189–208 (1983).
30. K. Karhunen, *Ann. Acad. Sci. Fenn. A1, Math. Phys.* **37** (1946).
31. M. Loève, *Fonctions aleatoires de second ordre*, C.R. Acad. Sci., Paris, France, 1946.
32. M. Hožič, and A. Stefanovska, *Physica A* **280**, 587–601 (2000).
33. M. T. Heideman, D. H. Johnson, and C. S. Burrus, *Rev. Mod. Phys.* **1**, 14–21 (1984).
34. C.-K. Peng, S. V. Buldyrev, S. Havlin, M. Simons, H. E. Stanley, and A. L. Goldberger, *Phys. Rev. E.* **49**, 1685–1689 (1994).
35. Y. Shiogai, A. Stefanovska, and P. McClintock, *Phys. Rep.* **488**, 51–110 (2010).
36. M. V. Berry, *J. Phys. A* **12**, 781–797 (1979).
37. G. Kaiser, *A Friendly Guide to Wavelets*, Birkhäuser, Cambridge, MA, USA, 1994.
38. J. Jamšek, A. Stefanovska, and P. V. E. McClintock, *Phys. Rev. E* **76**, 046221 (2007).
39. J. Jamšek, M. Paluš, and A. Stefanovska, *Phys. Rev. E* **81**, 036207 (2010).
40. L. W. Sheppard, A. Stefanovska, and P. V. E. McClintock, *Phys. Rev. E.* **83**, 016206 (2011).
41. L. W. Sheppard, A. Stefanovska, and P. V. E. McClintock, *Phys. Rev. E* **85**, 046205 (2012).
42. T. Stankovski, A. Duggento, P. V. E. McClintock, and A. Stefanovska, Inference of time–evolving coupled dynamical systems in the presence of noise (2012), (to be published).